

Superfluid-Mott insulator quantum phase transition in a cavity optomagnonic system

Qian Cao,¹ Lei Tan,^{1,2,*} and Wu-Ming Liu³

¹*Lanzhou Center for Theoretical Physics, Key Laboratory of Theoretical Physics of Gansu Province, Lanzhou University, Lanzhou, Gansu, 730000, China*

²*Key Laboratory for Magnetism and Magnetic Materials of the Ministry of Education, Lanzhou University, Lanzhou 730000, China*

³*Beijing National Laboratory for Condensed Matter Physics, Institute of Physics, Chinese Academy of Sciences, Beijing 100190, China*

The emerging hybrid cavity optomagnonic system is a very promising quantum information processing platform for its strong or ultrastrong photon-magnon interaction on the scale of micrometers in the experiment. In this paper, the superfluid-Mott insulator quantum phase transition in a two-dimensional cavity optomagnonic array system has been studied based on this characteristic. The analytical solution of the critical hopping rate is obtained by the mean field approach, second perturbation theory and Landau second order phase transition theory. The numerical results show that the increasing coupling strength and the positive detunings of the photon and the magnon favor the coherence and then the stable areas of Mott lobes are compressed correspondingly. Moreover, the analytical results agree with the numerical ones when the total excitation number is lower. Finally, an effective repulsive potential is constructed to exhibit the corresponding mechanism. The results obtained here provide an experimentally feasible scheme for characterizing the quantum phase transitions in a cavity optomagnonic array system, which will offer valuable insight for quantum simulations.

I. INTRODUCTION

Quantum simulation provides a useful tool for solving many problems such as quantum phase transition, quantum magnetism, and high-temperature superconductivity[1]. Quantum phase transition of an interaction system composed of multiple particles are widely investigated, such as heavy fermions in Kondo lattices[2], ultracold atoms in optical lattices [3–5], and the ensemble of two-level systems interacting with a bosonic field (i.e., Dicke model)[6]. Especially, the superfluid-Mott insulator quantum phase transition of bosons, which forms one of the paradigm examples of a quantum phase transition, was first studied in the Bose Hubbard (BH) model due to the competition of the on-site interaction and the hopping term theoretically and experimentally[7–10]. Given the precise control of coupling strengths, the properties of scalability and individual accessibility of coupled cavities[11–14], the Jaynes–Cummings Hubbard (JCH) model, which describes the dynamics of the coupled-cavity arrays with each embedded within a two-level atom has attracted tremendous attentions[15–17] in recent years. Based on the JCH model and extended JCH model, the superfluid-Mott insulator quantum phase transition of light reminiscent of the ones of atoms in the BH model are extensively simulated[18–26]. More importantly, the quantum phase transition of light depends crucially on the intrinsic atom-photon interaction in the JCH model, where the atom-photon coupling leads to the formation of repelled collective polaritonic excitations, and this on-site repulsive potential compete with the hopping of photons between neighbouring cavities. On the other hand, the quantum phase transition of light has great potential application for a new source of quantum-correlated photons[1, 23, 27–

30].

Hereafter, with the fabrication of optomechanical cavity systems at the desired frequency accuracy and the coupling strength, the cavity optomechanical array system provides another experimentally feasible avenue to simulate the superfluid-Mott insulator quantum phase transition[31–33]. Compared with coupled cavity arrays system, the phonon-mediated cavity field and the two-level system form polaritons by coupling, which provide an effective on-site repulsion, then the system can also simulate the superfluid-Mott insulator quantum phase transition. Interestingly, the enhanced phonon-photon coupling favors the coherence of the system[34].

In analogy to the cavity optomechanical system, cavity optomagnonic system, a new class of hybrid quantum systems based on collective spin excitations in ferromagnetic materials[35], has received increasing attention in recent years, which provides a new and promising platform for studying macroscopic quantum effects[35–43]. The collective spin excitation in ferromagnetic crystals is called a magnon, which can interact coherently with microwaves and optical photons as well as phonons via magnetic dipole, magneto-optical, and magnetostrictive interactions, respectively[44–47]. Experimentally, yttrium iron garnet (YIG) spheres are characterized with high collective spin excitation density, low dissipation, great frequency tunability and the longer coherence time, which are widely used in the study of magnon-photon coupling due to its strong and even ultrastrong couplings[48, 49, 35]. In addition, the strong coupling between cavity photon and magnon has been observed at both low and high temperature experimentally[50]. Based on these features of cavity optomagnonic system, many intriguing phenomena have been explored, such as magnon dark modes and gradient memory[51], coher-

ent and dissipative magnon-photon interaction[52–59], the high-order sideband generation[60], the self-sustained pscillations and chaos[61–63], non-Hermitian physics[55, 64, 65], entanglement[66–70], magnon-induced nearly perfect absorption[71], magnon Fock state[72], magnon squeezing[73] and so on. Recently, several novel progresses associated with the photon blockade in cavity optomagnonic system are also investigated[74, 75, 76]. We note that the interplay of the photon blockade and photon hopping is not considered. In view of the unique advantages of magnons, it is very interesting to further explore the superfluid-Mott insulator quantum phase transition of light in the hybrid macroscopic quantum interface of atoms, photons and magnons.

In this work, we will investigate whether there is a superfluid-Mott insulator quantum phase transition in a cavity optomagnonic array system. Compared with the JCH model, three new degrees of freedom were added by the inclusion of YIG spheres, and the effects of these three new degrees on the quantum phase transition were investigated. Firstly, the analytical solutions for low excitation number are obtained based on the mean field approximation, the second order perturbation theory and the Landau phase transition theory. Then, the phase diagrams are discussed numerically using the mean-field theory. Finally, the effective repulsive potential is presented to show the mechanism of the superfluid-Mott insulator transition.

This paper is organized as follows: in Sec. II, we describe a cavity optomagnonic array system used for studying the superfluid-Mott insulator quantum phase transition of light. Sec. III is devoted to discussing the analytical solutions of this system, and the numerical solutions are given in Sec. IV. Conclusions are made in Sec. V.

II. MODEL AND HAMILTONIAN

Consider a cavity optomagnonic system composed of a 2D array of identical coupled optomagnonic cavities, with each cavity containing a two-level atom (TLA) interacting with the photon mode (see Fig. 1). The total Hamiltonian ($\hbar = 1$) of the system can be written as

$$\hat{\mathcal{H}}_T = \sum_i \hat{H}_i^{cpm} - \sum_{i,j} \kappa_{ij} \hat{a}_i^\dagger \hat{a}_j - \sum_i \mu_i \hat{N}_i \quad (1)$$

$$\begin{aligned} \hat{H}_i^{cpm} = & \omega_c \hat{a}_i^\dagger \hat{a}_i + \omega_a \hat{\sigma}_i^\dagger \hat{\sigma}_i + \omega_m \hat{m}_i^\dagger \hat{m}_i \\ & + g_a (\hat{\sigma}_i \hat{a}_i^\dagger + \hat{\sigma}_i^\dagger \hat{a}_i) + G_m (\hat{m}_i \hat{a}_i^\dagger + \hat{m}_i^\dagger \hat{a}_i) \end{aligned} \quad (2)$$

where i, j are the indexes for the individual optomagnonic cavity and range over all nearest neighbors sites, the subscript T is the abbreviation of the total. Here, the cavity optomagnonic system is denoted as the superscript cpm for convenience. $\hat{a}_i^\dagger (\hat{a}_i)$ and $\hat{m}_i^\dagger (\hat{m}_i)$ are the photonic and magnonic creation (annihilation) operators, respectively. $\hat{\sigma}_i^\dagger (\hat{\sigma}_i)$ are the atomic raising

and lowering operators, respectively. $\hat{\mathcal{N}}_i = \sum_i \hat{N}_i = \sum_i (\hat{a}_i^\dagger \hat{a}_i + \hat{m}_i^\dagger \hat{m}_i + \hat{\sigma}_i^\dagger \hat{\sigma}_i)$ is the total polariton number operator[77, 78]. N_i is the total number of photonic, magnonic and atomic excitations of the i th site in the cavity optomagnonic system. From the commutation relationship between the total polariton number operator $\hat{\mathcal{N}}_i$ and the Hamiltonian $\hat{\mathcal{H}}_T$, one can find that $\hat{\mathcal{N}}_i$ is a conserved quantity. It is feasible to describe this model in the grand-canonical ensemble and the chemical potential is μ_i , which is the Lagrange multiplier in the grand-canonical ensemble ensuring the conservation of the total excitation number in the phase transition between the Mott insulator and superfluid phases. G_m (g_a) represents the coupling strength of cavity mode and magnon (atom), respectively. ω_a , ω_c and ω_m are the frequencies of cavity photon, atom and magnon respectively, where $\omega_m = \gamma H$, γ is gyromagnetic ratio and H is the modulated magnetic field, which can be given by the Holstein-Primakoff (H-P) transformation[35, 79, 80]. We introduce the detuning between the atom and the cavity, $\Delta_a = \omega_a - \omega_c$, and the detuning between the magnon mode and the cavity mode is $\Delta_m = \omega_m - \omega_c$. In addition, the second term of Eq. (1) denotes the photon hopping between the nearest-neighbor cavities with the hopping rate κ_{ij} . We assume the hopping rate of photons $\kappa_{ij} = \kappa$ between adjacent sites i and j . The chemical potential $\mu_i = \mu$ is the same for all optomagnonic cavities for simplicity.

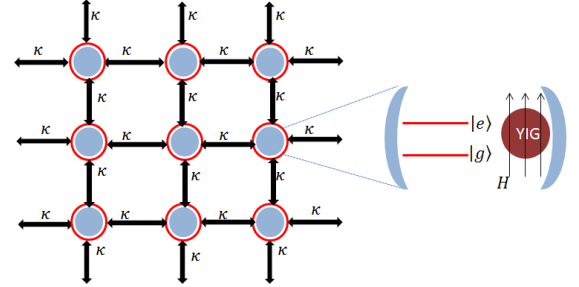


FIG. 1. Schematic diagram of a two-dimensional hybrid coupled optomagnonic cavity array setup. Each optomagnonic cavity contains a two-level atom and a YIG sphere is placed near the maximum magnetic field of the cavity mode and in a uniform bias magnetic field, which establishes the magnon-photon coupling.

We utilize the mean field approximation method to study the superfluid-Mott insulator quantum phase transition of light. In the mean field approximation, we introduce the superfluid order parameter $\psi \equiv \langle \hat{a}_i \rangle$ to study the quantum phase transition. Generally, ψ is a complex number, but its phase factor can be gauged away without affecting the Hamiltonian. Thus, ψ can be taken to be real in the present system. When $\psi = 0$, the system is in the Mott insulator phase. Otherwise, the system is in the superfluid phase. The boundary between $\psi = 0$ and $\psi \neq 0$ phases defines a quantum phase transition in the system. The final form Eq.(3) of the Hamiltonian is obtained by using the decoupling approximation, where

$z = 4$ is the number of nearest neighbours.

$$\mathcal{H}_T = \sum_i \left[H_i^{cpm} - z\kappa\psi (\hat{a}_i^\dagger + \hat{a}_i) - \mu N_i + z\kappa\psi^2 \right] \quad (3)$$

Therefore, we choose the eigenstates as the bare states of the cavity optomagnonic system, which is composed of the direct product of the cavity photon states, magnon states and atom states, i.e., $|\text{photon}(n), \text{magnon}(m), \text{atom}(e, g)\rangle$. The dimension of the subspace is $(2N+1) \times (2N+1)$. So, we choose a complete set of basis vectors $|N-m-1, m, e\rangle, |0, N-1, e\rangle, |N-m, m, g\rangle, |1, N-1, g\rangle, |0, N, g\rangle$ to give the matrix form of the Hamiltonian Eq. (4) after the mean field approximation with n running 0, 1, 2, to N , while m takes 0, 1, 2, ..., $N-2$. Therefore, the matrix dimension of $H_{(N)}^{MF}$ can be defined $(2N+1) \times (2N+1)$, and likewise, the matrix dimension of $H_{(N)}^{hop}$ is

defined as $(2N+1) \times (2(N+1)+1)$. The matrix expression can be obtained as follows. The superscript MF and hop are the abbreviation of the Mean field approximation and the hopping term respectively.

$$\mathcal{H}^{MF} = z\kappa\psi^2 I + \begin{pmatrix} H_{(0)}^{MF} & H_{(0)}^{hop} & 0 & 0 & 0 \\ H_{(0)}^{hopT} & H_{(1)}^{MF} & H_{(1)}^{hop} & 0 & 0 \\ 0 & H_{(1)}^{hopT} & H_{(2)}^{MF} & H_{(2)}^{hop} & 0 \\ 0 & 0 & H_{(2)}^{hopT} & H_{(3)}^{MF} & 0 \\ & & & \ddots & \ddots \\ 0 & 0 & 0 & 0 & H_{(N)}^{MF} \end{pmatrix} \quad (4)$$

$$H_{(N)}^{MF} = \begin{pmatrix} & & & \sqrt{N}g_a & 0 & 0 & 0 \\ & H_2 & & 0 & \sqrt{N-1}g_a & 0 & 0 \\ & & & 0 & 0 & \ddots & 0 \\ & & & 0 & 0 & & g_a \\ \sqrt{N}g_a & 0 & 0 & & & & \\ 0 & \sqrt{N-1}g_a & 0 & & & & \\ & & \ddots & & & & \\ 0 & 0 & & g_a & & & \\ 0 & 0 & 0 & 0 & & & \end{pmatrix}_{(2N+1) \times (2N+1)} \quad (5)$$

The specific forms of H_1 and H_2 are in the Appendix A.

$$H_{(N)}^{hop} = \begin{pmatrix} -\sqrt{N-1}z\kappa\psi & 0 & 0 & 0 & 0 & 0 & 0 \\ 0 & -\sqrt{N-2}z\kappa\psi & 0 & 0 & 0 & 0 & 0 \\ & & \ddots & & & & \\ 0 & 0 & 0 & -\sqrt{N}z\kappa\psi & 0 & 0 & 0 \\ 0 & 0 & 0 & 0 & -\sqrt{N-1}z\kappa\psi & 0 & 0 \\ & & & & \ddots & & \\ 0 & 0 & 0 & 0 & 0 & -z\kappa\psi & 0 \end{pmatrix}_{(2N+1) \times (2N+3)} \quad (6)$$

For example, when the total excitation number is $N = 0$ ($N = 1$), the basis vectors are selected as $|0, 0, g\rangle$ ($|1, 0, g\rangle, |0, 1, g\rangle, |0, 0, e\rangle$). And the matrix of $H_{(0)}^{MF} = (0)$ for $N = 0$. For $N = 1$, the matrix dimension of $H_{(1)}^{MF}$ should be substituted by

$$H_{(1)}^{MF} = \begin{pmatrix} \omega_a - \mu & g_a & 0 \\ g_a & \omega_c - \mu & G_m \\ 0 & G_m & \omega_m - \mu \end{pmatrix} \quad (7)$$

Introducing the detuning between the photon frequency and the two-level transition frequency Δ_a (magnon frequency Δ_m), the resulting Hamiltonian is

$$H_{(1)}^{MF'} = \begin{pmatrix} \Delta_a - \mu & g_a & 0 \\ g_a & \omega_c - \mu & G_m \\ 0 & G_m & \Delta_m - \mu \end{pmatrix} \quad (8)$$

the eigenvalues are given ($\Delta_a = \Delta_m = \Delta$)

$$E'_{1,0} = \Delta - \mu \quad (9)$$

$$E'_{1,-} = \frac{1}{2} \left(\Delta - 2\mu + \omega_c - \sqrt{\Delta^2 - 2\Delta\omega_c + 4g_a^2 + 4G_m^2 + \omega_c^2} \right) \quad (10)$$

$$E'_{1,+} = \frac{1}{2} \left(\Delta - 2\mu + \omega_c + \sqrt{\Delta^2 - 2\Delta\omega_c + 4g_a^2 + 4G_m^2 + \omega_c^2} \right) \quad (11)$$

The splitting between states with the same excitation number of a polariton is given by

$$\delta_E = E'_{1,-} - E'_{1,+} = \sqrt{\Delta^2 - 2\Delta\omega_c + 4g_a^2 + 4G_m^2 + \omega_c^2} \quad (12)$$

Note that, the splitting δ_E does not only depend on the detunings of the photon-atom and the photon-magnon but also depend on their coupling strengths. That is to say, in a cavity optomagnonic system, the strong photon-magnon and photon-atom coupling are all involved in

the polariton mapping[77]. Meantime, three new degrees of freedom are added in the new model compared with JCH model, which are the excitation number m of the magnon, the coupling strength G_m and the detuning Δ_m between the cavity field and the magnon. From the above discussion, we can determine that the excitation number of the magnon (m) is constrained by the total excitation number (N). In the following section, we will first deduce the analytical expressions for the order parameter and the critical hopping rate based on the second-order perturbation method and the Landau theory for the continuous phase transitions.

III. ANALYTICAL SOLUTIONS

To get the simple analytical expression, we assume that the cavity frequency, atomic frequency, and magnon frequency are the same, i.e. $\omega_m = \omega_c = \omega_a \equiv \omega$. Considering Eq. (5) for lower excitations without the hopping term, the eigenvalues are given in Appendix B.

Then we need to think about the eigenstates that correspond to each eigenvalue. Here, we take $E_{1,-}$, $E_{2,-}$ as examples to obtain the analytical solutions of the order parameter for the quantum phase transition. The expressions of the corresponding eigenstate are

$$\phi_1 \equiv \frac{1}{\sqrt{B_1}} (|0, 1, g\rangle + a_1 |1, 0, g\rangle + d_1 |0, 0, e\rangle) \quad (13)$$

$$\phi_2 \equiv \frac{1}{\sqrt{B_2}} (|0, 2, g\rangle + a |1, 0, e\rangle + b |0, 1, e\rangle + c |2, 0, g\rangle + d |1, 1, g\rangle) \quad (14)$$

The ground state is $\phi_0 = |0, 0, g\rangle$, and the parameters involved in Eqs. (13)-(14) are detailed in Eqs. (B10)-(B17).

The second order perturbation theory is a commonly used method to study the analytical solution of the superfluid-Mott insulator quantum phase transition[15, 81]. Therefore, we take the hopping term H^{hop} as the perturbation term and calculate the analytical solution of the system. One can get the second-order corrections to the energy and the normalized eigenstates are shown in Eqs. (B18)-(B22).

Then, according to the second-order perturbation theory, we can write the approximative wave function as

$$\Phi = \frac{1}{\sqrt{N_t}} (\phi_1^{(0)} + \phi_1^{(1)}), \text{ where } N_t = 1 + \frac{|\langle \phi_2^{(0)} | \hat{a}^\dagger | \phi_1^{(0)} \rangle|^2}{(E_{1,-}^{(0)} - E_{2,-}^{(0)})^2} + \frac{|\langle \phi_0^{(0)} | \hat{a} | \phi_1^{(0)} \rangle|^2}{(E_{1,-}^{(0)} - E_{0,0}^{(0)})^2} \text{ is a normalization coefficient.}$$

Based on the definition formula of the order parameter ψ and the wave function Φ , the analytical formula of the order parameter ψ can be given

$$\psi = \sqrt{\frac{\frac{-z\kappa |\langle \phi_2^{(0)} | \hat{a}^\dagger | \phi_1^{(0)} \rangle|^2}{E_{1,-}^{(0)} - E_{2,-}^{(0)}} - \frac{z\kappa |\langle \phi_0^{(0)} | \hat{a} | \phi_1^{(0)} \rangle|^2}{E_{1,-}^{(0)} - E_{0,0}^{(0)}} - 1}{\frac{z\kappa |\langle \phi_2^{(0)} | \hat{a}^\dagger | \phi_1^{(0)} \rangle|^2}{(E_{1,-}^{(0)} - E_{2,-}^{(0)})^2} + \frac{z\kappa |\langle \phi_0^{(0)} | \hat{a} | \phi_1^{(0)} \rangle|^2}{(E_{1,-}^{(0)} - E_{0,0}^{(0)})^2}}} \quad (15)$$

Furthermore, the expansion of the energy in power series in ψ can be given by

$$E_{1,-} = E_{1,-}^{(0)} + E_{1,-}^{(2)} + z\kappa\psi^2 + O(\psi^4) \quad (16)$$

$E_{1,-}^{(2)}$ is given by Eq. (B8).

Hereafter, according to Landau's second-order phase transition theory, the phase boundary of the Mott insulator phase and the superfluid phase can be determined when the coefficient of the square term ψ is zero[82, 83]. Then, the critical hopping rate κ_c can be acquired. The system hold the Mott insulator state when $\kappa < \kappa_c$, and in other cases, the system is in a superfluid state. Based on these expressions, the boundaries between the superfluid phase and the Mott insulator phase with the different coupling strength G_m are shown in Figs. 4(e)-4(f), and the specific analysis will be discussed in the next Section.

$$z\kappa_c = \begin{cases} \frac{B_1 E_{1,-}}{a_1^2} & N = 0; \\ \frac{-(E_{1,-}^{(0)} - E_{2,-}^{(0)}) E_{1,-}^{(0)}}{|\langle \phi_2^{(0)} | \hat{a}^\dagger | \phi_1^{(0)} \rangle|^2 E_{2,-}^{(0)} + |\langle \phi_0^{(0)} | \hat{a} | \phi_1^{(0)} \rangle|^2 (E_{1,-}^{(0)} - E_{2,-}^{(0)})} & N = 1; \end{cases} \quad (17)$$

Up till now, the order parameter ψ and the critical hopping rate are obtained based on a mean-field theory in order to analyze the quantum phase transition of the system. In what follows, we will use a numerical method to discuss the behaviors of the superfluid-Mott insulator quantum phase transition and compare with the analytical results mentioned above against the controlling parameters of our model.

IV. MOTT-SUPERFLUID TRANSITION

We first investigate the critical chemical potential as a function of Δ_a , which is usually defined as $E_{N+1,-} - \mu(n+1) = E_{N,-} - \mu n$. Figure 2 exhibits the change of boundaries between different Mott lobes for various detuning Δ_m . Meanwhile, the analytic solution between states $|0, 0, -\rangle$ and $|1, 0, -\rangle$ is also shown in Fig. 2(a). Obviously, the analytic solutions are conformed with the numerical solution on the lower excitation number. Figures 2(a)-2(e) also show the Mott lobes with different Δ_m , which exhibit that the Mott lobes are smaller and closer with $|\Delta_a/g_a|$ increasing. That's means that the regions of stability become observably smaller with the excitation number and the detuning $|\Delta_a/g_a|$ increasing and it's easy to notice that the states $|0, 0, -\rangle$ and $|1, 0, -\rangle$ are the most stable ones in Figs. 2(a)-2(e). The phase boundary between the lowest and the second lowest states with different Δ_m is shown in Fig. 2(f), which illustrates that the stable region of state $|0, 0, -\rangle$ becomes large with Δ_m increasing. In addition, it can be found that the Mott lobes are asymmetric with respect to Δ_a , which is different compared with JCH model[15]. This means that the phase boundaries at higher excitation are also asymmetric with respect to Δ_a . Compared Figs. 2(b)-2(c) with Figs. 2(d)-2(e), it can also be found that the stable regions for a negative detuning is smaller than ones of the positive detuning.

Figure 3 show the critical chemical potential as a function of Δ_a for different coupling strength G_m/g_a . As

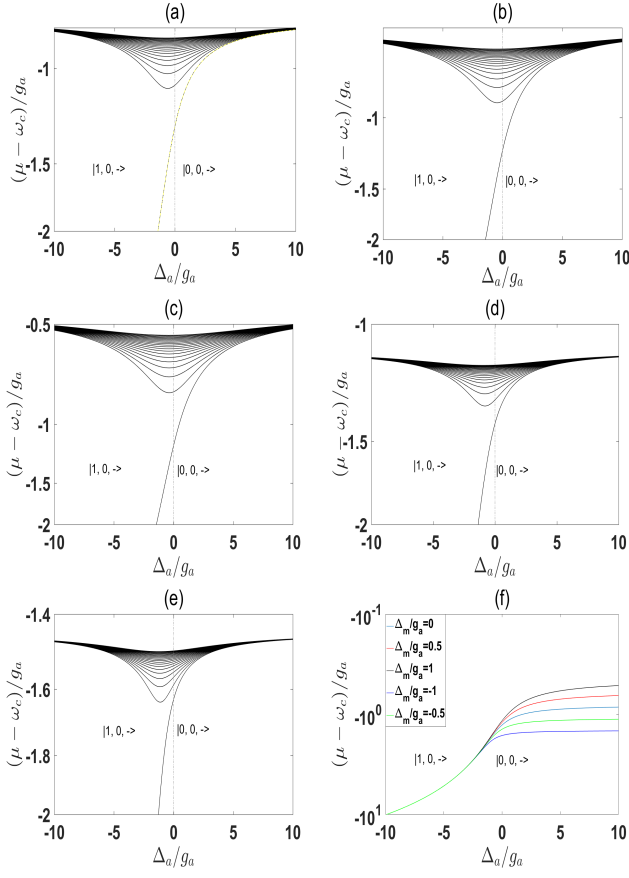


FIG. 2. Boundaries between different Mott lobes as a function of μ and Δ_a when the hopping rate approaches zero for different Δ_m with $G_m/g_a = 0.8$. (a) $\Delta_m = 0$, The yellow dashed line is the analytical result between states $|0, 0, -\rangle$ and $|1, 0, -\rangle$. (b) $\Delta_m = 0.5$, (c) $\Delta_m = 1$, (d) $\Delta_m = -0.5$, (e) $\Delta_m = -1$. And (f) exhibits the boundary between states $|0, 0, -\rangle$ and $|1, 0, -\rangle$ for different Δ_m .

shown in Figs. 3(a)-3(d), the Mott lobes get smaller and closer together with increasing $|\Delta_a/g_a|$, which means that the stable area decreases with $|\Delta_a/g_a|$ increasing. At the same time, the stable area decreases with the increase of the total excitation number, which can be observed in Figs. 3(a)-3(d). However, it is easy to see that all Mott lobes are symmetric with respect to the detuning Δ_a , except for the states between $|0, 0, -\rangle$ and $|1, 0, -\rangle$ according to Fig. 3(a), which means that the phase boundary at higher excitation number is symmetric only when $G_m/g_a = 0$. Furthermore, the stable region of state $|0, 0, -\rangle$ decreases with increasing of the coupling strength G_m/g_a as shown in Fig. 3(e).

After investigating the boundaries between different Mott lobes within the dressed-state formalism in our system, we will calculate the phase diagram by applying the mean-field theory. The well-known feature of the superfluid-Mott insulator quantum phase transition is the Mott lobe which is exhibited in Fig. 4 for different values of G_m with a cutoff $N = 20$ to the total excitation

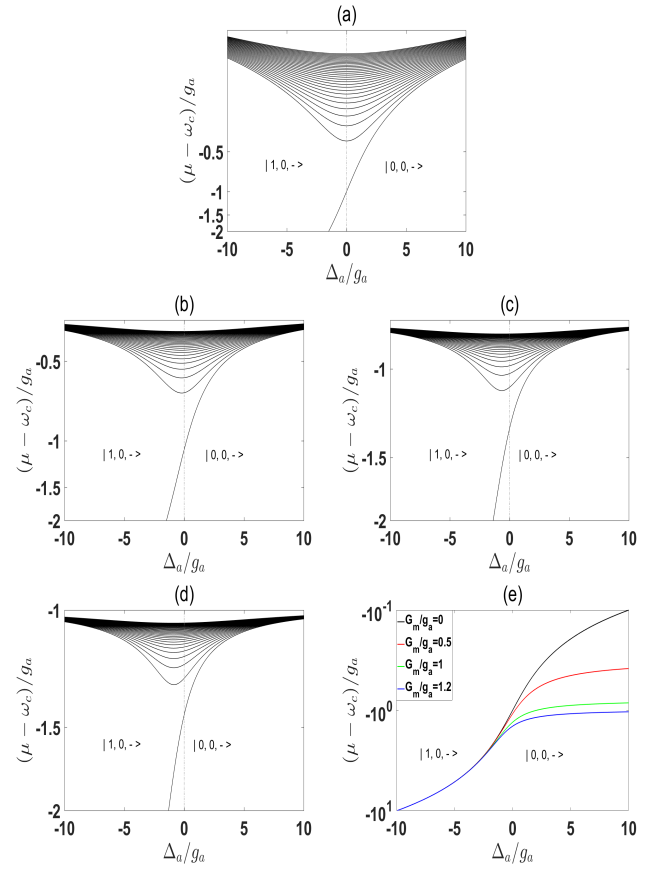


FIG. 3. Boundaries between Mott lobes as a function of μ and Δ_a when the hopping rate approaches zero for different G_m with $\Delta_m = 0.5$. (a) $G_m/g_a = 0$. (b) $G_m/g_a = 0.5$, (c) $G_m/g_a = 1$, and (d) $G_m/g_a = 1.2$, and (e) exhibits the boundary between states $|0, 0, -\rangle$ and $|1, 0, -\rangle$ with different G_m/g_a .

number basis so that $0 < m < N$. Note that, without photon-magnon interaction in Eqs.(1)-(2), i.e., $G_m = 0$, the hybrid system considered here can be reduced to the usual JCH model. In order to make a comparison with the cases discussed below, the phase diagram for the JCH model is also plotted in Fig. 4(a). One can easily find the superfluid-Mott insulator quantum phase transition that the parameter space is separated into two distinct phases as shown in Figs. 4(b)- 4(d). There are clearly the superfluid phase corresponding to the regions where $\psi \neq 0$ for large hopping rate κ , and the stable ground state of each site is a coherent state. The Mott insulator phase corresponds to the case of $\psi = 0$ for a small hopping rate κ . Each Mott lobe corresponds to a state with an integer number of the total excitations per site. Compared Figs. 4(b)- 4(d) with Fig. 4(a), one can find that a small hopping rate is needed to delocalize the photons and make them enter the superfluid phase. Additionally, the enhanced photon-magnon coupling strength G_m causes the region of each Mott lobe to decrease and the superfluid phase area is increased with the increasing of

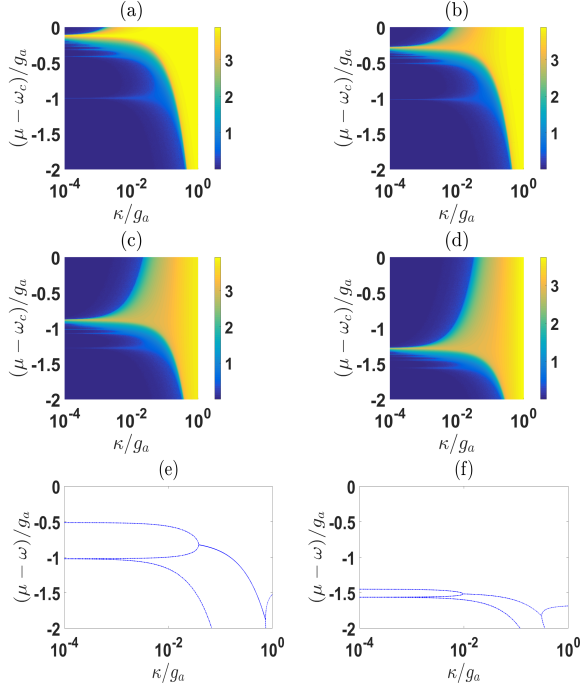


FIG. 4. The superfluid order parameter as a function of the photon hopping rate κ and the chemical potential μ for different coupling strengths G_m with $\Delta_m = \Delta_a = 0$. (a) $G_m/g_a = 0$, (b) $G_m/g_a = 0.2$, (c) $G_m/g_a = 0.8$, (d) $G_m/g_a = 1.2$. (e)-(f) Analytical boundaries between different phases as a function of $\mu - \omega_c$ and κ/g_a with $\Delta_a = \Delta_m = 0$. (e) $G_m = 0.2$, (f) $G_m = 1.2$.

G_m correspondingly. These results mean that the coupling of the photon-magnon favors the superfluid phase, which is consistent with the results shown in Fig. 3. Furthermore, the analytical results based on Eq. (17) are also shown in Figs. 4(e)-4(f), which are described by the blue dashed contours. As expected, we find well agreement between this analytical calculation and the full mean-field calculation in determining the boundary between the superfluid and the Mott insulator phase when the hopping rate is weak. By comparing Fig. 4(e) (4(f)) with Fig. 4(b) (4(d)), the analytical results obtained from the second-order perturbation theory are no longer applicable at large hopping rate.

According to the H-P transformation, the magnon frequency can be regulated by a bias magnetic field[35, 79, 80]. Therefore, the detuning Δ_m between the cavity photon and the magnon can be used as an experimentally feasible parameter for adjusting the superfluid-Mott insulator quantum phase transition. Figure 5 exhibits the change of the phase diagram for different detuning Δ_m . Figures 5(a), 5(c) and 5(e) show that the region of each Mott lobe does not change significantly but tends to increase slightly for the detuning Δ_m positive increasing. While for a negative detuning, i.e., $\Delta_m < 0$, the effect on the transition of the superfluid-Mott insulator can be enhanced as shown in Figs. 5(b) and 5(d). It can be found

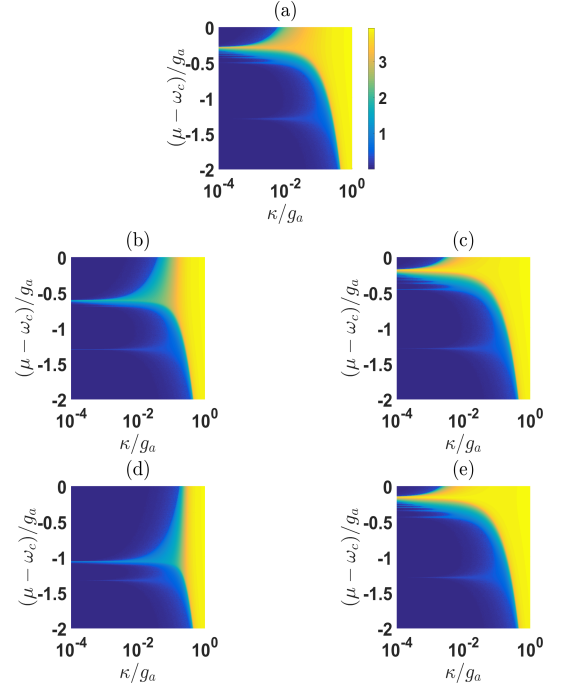


FIG. 5. The superfluid order parameter as a function of the photon hopping rate κ and the chemical potential μ for different detuning of magnon and cavity photon Δ_m with $G_m = 0.2, \Delta_a = 0.5$. (a) $\Delta_m/g_a = 0$, (b) $\Delta_m/g_a = -0.5$, (c) $\Delta_m/g_a = 0.5$, (d) $\Delta_m/g_a = -1$, (e) $\Delta_m/g_a = 1$.

that the detunings decreases not only reduce the area of the Mott lobe, but also have a tendency to diminish the Mott lobe with large total excitation number N . Then it is more favorable for the generation of highly excited Mott lobes when Δ_m is positive.

In order to determine the excitation numbers corresponding to each Mott lobe in the phase diagram. We plot the average excitations number $\langle N \rangle$ and the average photon (magnon) number $\langle n \rangle$ ($\langle m \rangle$) per site for the normalized chemical potential $(\mu - \omega_c)/g_a$ in Fig. 6 for $N = 20$. It is easy to see that the evolutions of $\langle N \rangle$, $\langle n \rangle$, $\langle m \rangle$ reflect a conspicuous staircase due to the competition between diverse ground-states, and accordingly, each Mott lobe in the phase diagram is characterized by the corresponding plateaus. Figure 6 also exhibits $\langle N \rangle$, $\langle n \rangle$ and $\langle m \rangle$ for different coupling strengths G_m and detunings Δ_m . It is easy to notice that the enhanced photon-magnon coupling strength G_m leads to a increase of the average magnon number $\langle m \rangle$ per site and a decrease of the average photon number $\langle n \rangle$ per site correspondingly. It is not difficult to understand that the large detuning Δ_m can cause the photon-magnon coupling to become weaker and thus reduces the excitation of the magnons. Therefore, with increasing Δ_m , the average number of magnons tends to decrease as shown in Fig. 6(b).

In general, the superfluid-Mott insulator quantum phase transition can partly be understood by the competition arising from the effective on-site repulsive potential

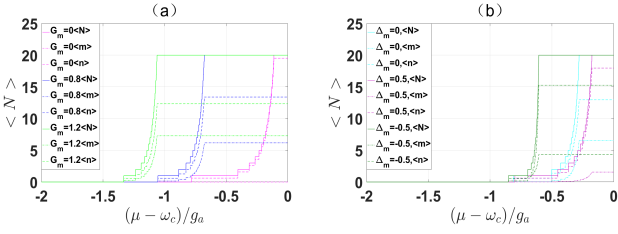


FIG. 6. The average excitations number $\langle N \rangle$ (photon number $\langle n \rangle$ and magnon number $\langle m \rangle$) as a function of the normalized chemical potential $(\mu - \omega_c)/g_a$ for different detunings and photon-magnon coupling strength. (a) $\Delta_a/g_a = \Delta_m/g_a = 0.5$. (b) $\Delta_a/g_a = 0.5, G_m/g_a = 0.2$.

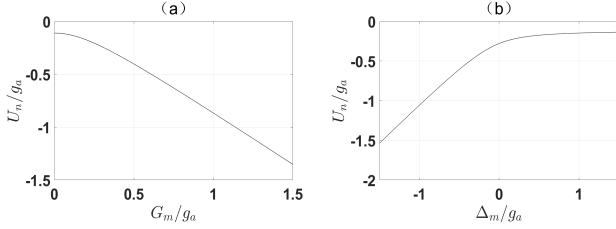


FIG. 7. (a) Show the normalized effective repulsive potential U_n versus the cavity-magnon coupling strength G_m/g_a . (b) Show the normalized effective repulsive potential U_n as a function of the detuning Δ_m/g_a . Other parameters are the same as in Fig. 4 and Fig. 5.

and the photon hopping. As the effective on-site repulsive potential dominates the hopping rate, the system should be in a Mott insulator phase; on the contrary, the system is in a superfluid state. The effective on-site repulsive potential U_n can be defined as $U_n = E_{N+1,-} - E_{N,-} - \omega_c$. Figure. 7(a) shows the effective on-site repulsive potential U_n for the coupling strength G_m . Obviously, U_n decreases with the increase of G_m . Thus, for a strong photon-magnon coupling, the diminished effective on-site repulsive potential leads the system tend to be more delocalized for a certain hopping rate. Then, the superfluid region increases accordingly as shown in Fig. 4. One can also notice that U_n increases with the increase of detuning Δ_m , which leads the Mott insulator phase area increase corresponding to Fig. 5.

V. CONCLUSION AND DISCUSSION

In conclusion, we have investigated the superfluid-Mott insulator quantum phase transition of light in a two-dimensional cavity optomagnonic array system. Firstly, the critical hopping rate of lower excitations is obtained by the second perturbation theory and Landau second-order phase transition theory. In addition, the phase boundaries between the Mott insulator phase and the superfluid phase are given accordingly the critical hopping

rate, and these results are consistent with the numerical ones when the hopping rate is weak. The coupling strength is favorable to the superfluid phase, and the stable region of the Mott lobe decreases with the increase of the photon-magnon coupling strength. Finally, the complete and stable phase diagram is exhibited on the positive photon-magnon detuning, and the highly excited Mott lobe tends to disappear when the detuning is negative. The effective on-site repulsive potential can explain these results. Additionally, our work may extend the studies based on the cavity optomagnonic system and offer a novel idea to explore the superfluid-Mott insulator quantum phase transition of light.

Experimentally, it is a mature technology that a strong coupling magnon-photon system can be engineered in experiments[42, 64, 80, 84,85]. In addition, the system of a two-level superconducting flux qubit, playing the role of an artificial atom, coupled with the cavity mode has also been realized in experiments[86]. And the linear array of 3D cavities and qubits for experiments has been developed[87]. Then, the theoretical model proposed here may be experimentally realized if one integrates the processes of the three points mentioned above. For simplicity, the parameters are scaled by g_a for numerical results. According to the theoretical results obtained here, the parameters values for superfluid-Mott insulator quantum phase transition of light will vary for different conditions. To observe these phenomena, the range of parameters is as follows: the coupling strength between photon and magnon $G_m/2\pi$ is 0 to 180MHz, the detuning of photon-magnon Δ_m is -0.942GHz to 0.942GHz , and the hopping rate κ is 94.2kHz to $28 \times 10^3\text{kHz}$ [86, 88], which can be achievable in cavity optomagnonic system experimentally. Furthermore, the disorder of this system induces some interesting effects for the quantum phase transition. Taking the JCH model as an example, the disorder of the light-matter interaction and the disorder of detuning between light-matter both induce the transition superfluid phase to the Mott insulator phase, and the disorder in the hopping induces a glassy fluid phase[89]. On the other hand, the effects of the tiny disorder and the weak fluctuations due to temperature can be suppressed by the excitation-hole gap in the Mott-insulator region, then the Mott phase are robustness and should be possible in the considering system[15].

VI. ACKNOWLEDGMENTS

This work was supported by National Natural Science Foundation of China (Grants No. 11874190, No. 61835013 and No. 12047501), and National Key R&D Program of China under grants No. 2016YFA0301500. Support was also provided by Supercomputing Center of Lanzhou University.

- * tanlei@lzu.edu.cn
- ¹ I. M. Georgescu, S. Ashhab, and F. Nori, *Rev. Mod. Phys.* **86**, 153 (2014).
 - ² H. v. Löhneysen, A. Rosch, M. Vojta, and P. Wölfle, *Rev. Mod. Phys.* **79**, 1015 (2007).
 - ³ E. Altman, W. Hofstetter, E. Demler, and M. D. Lukin, *New Journal of Physics* **5**, 113 (2003).
 - ⁴ J.-R. Han, T. Zhang, Y.-Z. Wang, and W. Liu, *Physics Letters A* **332**, 131 (2004).
 - ⁵ P. P. Orth, I. Stanic, and K. Le Hur, *Phys. Rev. A* **77**, 051601 (2008).
 - ⁶ R. H. Dicke, *Phys. Rev.* **93**, 99 (1954).
 - ⁷ M. P. A. Fisher, P. B. Weichman, G. Grinstein, and D. S. Fisher, *Phys. Rev. B* **40**, 546 (1989).
 - ⁸ D. Jaksch, C. Bruder, J. I. Cirac, C. W. Gardiner, and P. Zoller, *Phys. Rev. Lett.* **81**, 3108 (1998).
 - ⁹ S. Sachdev, *Quantum Phase Transitions*, by Subir Sachdev, Cambridge, UK: Cambridge University Press, 2011 (2011), 10.1017/CBO9780511622540.
 - ¹⁰ M. O. E. T. B.-T. W. H.-I. Greiner, Markus, *Nature* **415**, 39.
 - ¹¹ W. C. E. M.-C. M. B.-I. K. S. Sherson, Jacob F., *Nature* **467**, 68.
 - ¹² K. M. Gheri and H. Ritsch, *Phys. Rev. A* **56**, 3187 (1997).
 - ¹³ C. J. M. G. J. M. B. L. S. S. D. I. M. J. B. A. F. L. G. S. M. S. R. J. DiCarlo, L., *Nature* **460**, 240.
 - ¹⁴ S. Olmschenk, K. C. Younge, D. L. Moehring, D. N. Matsukevich, P. Maunz, and C. Monroe, *Phys. Rev. A* **76**, 052314 (2007).
 - ¹⁵ C. J. H. G. A. D. Tahan, Charles and L. C. L. Hollenberg, *Nature Physics* **2**, 856 (2006).
 - ¹⁶ B. a. P. M. B. C. J. H. G. A. D. Hartmann, Michael J. and L. C. L. Hollenberg, *Nature Physics* **2**, 849 (2006).
 - ¹⁷ D. G. Angelakis, M. F. Santos, and S. Bose, *Phys. Rev. A* **76**, 031805 (2007).
 - ¹⁸ R. Lin, C. Georges, J. Klinder, P. Mognini, M. Bttner, A. U. J. Lode, R. Chitra, A. Hemmerich, and H. Keßler, “Mott transition in a cavity-boson system: A quantitative comparison between theory and experiment,” (2021), [arXiv:2104.11253 \[cond-mat.quant-gas\]](https://arxiv.org/abs/2104.11253).
 - ¹⁹ B. Song, S. Dutta, S. Bhave, J.-C. Yu, E. Carter, N. Cooper, and U. Schneider, “Realizing discontinuous quantum phase transitions in a strongly-correlated driven optical lattice,” (2021), [arXiv:2105.12146 \[cond-mat.quant-gas\]](https://arxiv.org/abs/2105.12146).
 - ²⁰ X. Zhu, J. Guo, N. P. Breuckmann, H. Guo, and S. Feng, “Quantum phase transitions of interacting bosons on hyperbolic lattices,” (2021), [arXiv:2103.15274 \[cond-mat.str-el\]](https://arxiv.org/abs/2103.15274).
 - ²¹ H. Chen and X. C. Xie, *Physical Review B* **103** (2021), 10.1103/physrevb.103.205144.
 - ²² Q. Huang, R. Yao, L. Liang, S. Wang, Q. Zheng, D. Li, W. Xiong, X. Zhou, W. Chen, X. Chen, and J. Hu, “Observation of many-body quantum phase transitions beyond the kibble-zurek mechanism,” (2020), [arXiv:2012.01734 \[quant-ph\]](https://arxiv.org/abs/2012.01734).
 - ²³ K. Kamide, M. Yamaguchi, T. Kimura, and T. Ogawa, *Phys. Rev. A* **87**, 053842 (2013).
 - ²⁴ C. B. Gomes, A. M. C. Souza, and F. A. G. Almeida, “Mott insulator to superfluid phase transition in bravais lattices via the jaynes-cummings-hubbard model,” (2012), [arXiv:1211.5515 \[cond-mat.str-el\]](https://arxiv.org/abs/1211.5515).
 - ²⁵ O. O. Soykal and C. Tahan, *Phys. Rev. B* **88**, 134511 (2013).
 - ²⁶ L.-L. Zheng, K.-M. Li, X.-Y. Lü, and Y. Wu, *Phys. Rev. A* **96**, 053809 (2017).
 - ²⁷ C. Noh and D. G. Angelakis, *Reports on Progress in Physics* **80**, 016401 (2016).
 - ²⁸ S. Schmidt and J. Koch, *Annalen der Physik* **525**, 395 (2013).
 - ²⁹ A. A. Houck, H. E. Türeci, and J. Koch, *Nature Physics* **8** (2012), 10.1103/PhysRevLett.123.246801.
 - ³⁰ M. Hartmann, F. Brandão, and M. Plenio, *Laser & Photonics Reviews* **2**, 527 (2008).
 - ³¹ A. Mari, A. Farace, N. Didier, V. Giovannetti, and R. Fazio, *Phys. Rev. Lett.* **111**, 103605 (2013).
 - ³² M. Zhang, S. Shah, J. Cardenas, and M. Lipson, *Phys. Rev. Lett.* **115**, 163902 (2015).
 - ³³ V. Peano, C. Brendel, M. Schmidt, and F. Marquardt, *Phys. Rev. X* **5**, 031011 (2015).
 - ³⁴ Q. L. H.-Q. G. W.-M. L. Jin-Lou Ma, Lei Tan, *J. Phys. B* **53**, 195402.
 - ³⁵ D. Lachance-Quirion, Y. Tabuchi, A. Gloppe, K. Usami, and Y. Nakamura, *Applied Physics Express* **12**, 070101 (2019).
 - ³⁶ C. Zhao, X. Li, S. Chao, R. Peng, C. Li, and L. Zhou, *Phys. Rev. A* **101**, 063838 (2020).
 - ³⁷ A. Osada, R. Hisatomi, A. Noguchi, Y. Tabuchi, R. Yamazaki, K. Usami, M. Sadgrove, R. Yalla, M. Nomura, and Y. Nakamura, *Phys. Rev. Lett.* **116**, 223601 (2016).
 - ³⁸ Y.-P. Gao, X.-F. Liu, T.-J. Wang, C. Cao, and C. Wang, *Phys. Rev. A* **100**, 043831 (2019).
 - ³⁹ J. A. Haigh, A. Nunnenkamp, A. J. Ramsay, and A. J. Ferguson, *Phys. Rev. Lett.* **117**, 133602 (2016).
 - ⁴⁰ X. Zhang, C.-L. Zou, L. Jiang, and H. X. Tang, *Phys. Rev. Lett.* **113**, 156401 (2014).
 - ⁴¹ X. Zhang, N. Zhu, C.-L. Zou, and H. X. Tang, *Phys. Rev. Lett.* **117**, 123605 (2016).
 - ⁴² Y. Tabuchi, S. Ishino, T. Ishikawa, R. Yamazaki, K. Usami, and Y. Nakamura, *Phys. Rev. Lett.* **113**, 083603 (2014).
 - ⁴³ M. Goryachev, W. G. Farr, D. L. Creedon, Y. Fan, M. Kostylev, and M. E. Tobar, *Phys. Rev. Applied* **2**, 054002 (2014).
 - ⁴⁴ C. Kittel, *Phys. Rev.* **110**, 836 (1958).
 - ⁴⁵ K. P. Sinha and U. N. Upadhyaya, *Phys. Rev.* **127**, 432 (1962).
 - ⁴⁶ Y. R. Shen and N. Bloembergen, *Phys. Rev.* **143**, 372 (1966).
 - ⁴⁷ S. Demokritov, B. Hillebrands, and A. Slavin, *Physics Reports* **348**, 441 (2001).
 - ⁴⁸ C. A. V. Hillebrands, B., *Nature Physics* **11**, 453.
 - ⁴⁹ H. Tan and J. Li, *Phys. Rev. Research* **3**, 013192 (2021).
 - ⁵⁰ Y. Xiao, X. H. Yan, Y. Zhang, V. L. Grigoryan, C. M. Hu, H. Guo, and K. Xia, *Phys. Rev. B* **99**, 094407 (2019).
 - ⁵¹ Z. C.-L. Z. N. J.-L. T. H. X. C. J. H. G. A. D. Zhang, Xufeng and L. C. L. Hollenberg, *Nature Communications* **6**, 8914 (2015).
 - ⁵² D. Lachance-Quirion, Y. Tabuchi, A. Gloppe, K. Usami, and Y. Nakamura, *Applied Physics Express* **12**, 070101 (2019).
 - ⁵³ R. Hisatomi, A. Osada, Y. Tabuchi, T. Ishikawa, A. Noguchi, R. Yamazaki, K. Usami, and Y. Nakamura,

- Phys. Rev. B **93**, 174427 (2016).
- ⁵⁴ S. Viola Kusminskiy, H. X. Tang, and F. Marquardt, *Phys. Rev. A* **94**, 033821 (2016).
- ⁵⁵ M. Harder, Y. Yang, B. M. Yao, C. H. Yu, J. W. Rao, Y. S. Gui, R. L. Stamps, and C.-M. Hu, *Phys. Rev. Lett.* **121**, 137203 (2018).
- ⁵⁶ V. L. Grigoryan, K. Shen, and K. Xia, *Phys. Rev. B* **98**, 024406 (2018).
- ⁵⁷ Y.-P. Wang, J. W. Rao, Y. Yang, P.-C. Xu, Y. S. Gui, B. M. Yao, J. Q. You, and C.-M. Hu, *Phys. Rev. Lett.* **123**, 127202 (2019).
- ⁵⁸ W. Yu, J. Wang, H. Y. Yuan, and J. Xiao, *Phys. Rev. Lett.* **123**, 227201 (2019).
- ⁵⁹ Y.-P. Wang, J. W. Rao, Y. Yang, P.-C. Xu, Y. S. Gui, B. M. Yao, J. Q. You, and C.-M. Hu, *Phys. Rev. Lett.* **123**, 127202 (2019).
- ⁶⁰ W.-L. Xu, Y.-P. Gao, T.-J. Wang, and C. Wang, *Opt. Express* **28**, 22334 (2020).
- ⁶¹ S. Viola Kusminskiy, H. X. Tang, and F. Marquardt, *Phys. Rev. A* **94**, 033821 (2016).
- ⁶² Y.-P. Gao, C. Cao, Y.-W. Duan, X.-F. Liu, T.-T. Pang, T.-J. Wang, and C. Wang, *Nanophotonics* **9**, 1953 (2020).
- ⁶³ W.-L. Xu, X.-F. Liu, Y. Sun, Y.-P. Gao, T.-J. Wang, and C. Wang, *Phys. Rev. E* **101**, 012205 (2020).
- ⁶⁴ L. X.-Q. W. Y.-P.-L. T.-F. Y. Y. J. Q. Zhang, Dengke, *Nature Communications* **8**, 1368 (2017).
- ⁶⁵ G.-Q. Zhang and J. Q. You, *Phys. Rev. B* **99**, 054404 (2019).
- ⁶⁶ D. Kong, X. Hu, L. Hu, and J. Xu, *Phys. Rev. B* **103**, 224416 (2021).
- ⁶⁷ J. Li, S.-Y. Zhu, and G. S. Agarwal, *Phys. Rev. Lett.* **121**, 203601 (2018).
- ⁶⁸ Z.-B. Yang, H. Jin, J.-W. Jin, J.-Y. Liu, H.-Y. Liu, and R.-C. Yang, *Phys. Rev. Research* **3**, 023126 (2021).
- ⁶⁹ H. Tan and J. Li, *Phys. Rev. Research* **3**, 013192 (2021).
- ⁷⁰ J. Li and S.-Y. Zhu, *New Journal of Physics* **21**, 085001 (2019).
- ⁷¹ X.-P. C. G.-Y. S. W.-Y. P. Y. Y. Y. B. D. J. Rao, J. W., *Nature Communications* **12**, 1933 (2021).
- ⁷² V. A. S. V. Bittencourt, V. Feulner, and S. V. Kusminskiy, *Phys. Rev. A* **100**, 013810 (2019).
- ⁷³ J. Li, S.-Y. Zhu, and G. S. Agarwal, *Phys. Rev. A* **99**, 021801 (2019).
- ⁷⁴ C. Zhao, X. Li, S. Chao, R. Peng, C. Li, and L. Zhou, *Phys. Rev. A* **101**, 063838 (2020).
- ⁷⁵ Y.-P. Gao, X.-F. Liu, T.-J. Wang, C. Cao, and C. Wang, *Phys. Rev. A* **100**, 043831 (2019).
- ⁷⁶ F. Zou, D.-G. Liao, and J.-Q. Liao, *Optics express* **28**, 16175 (2020).
- ⁷⁷ C. Nietner, (2010).
- ⁷⁸ M. Hohenadler, M. Aichhorn, L. Pollet, and S. Schmidt, *Phys. Rev. A* **85**, 013810 (2012).
- ⁷⁹ T. Holstein and H. Primakoff, *Phys. Rev.* **58**, 1098 (1940).
- ⁸⁰ H. Huebl, C. W. Zollitsch, J. Lotze, F. Hocke, M. Greifenstein, A. Marx, R. Gross, and S. T. B. Goennenwein, *Phys. Rev. Lett.* **111**, 127003 (2013).
- ⁸¹ D. van Oosten, P. van der Straten, and H. T. C. Stoof, *Phys. Rev. A* **63**, 053601 (2001).
- ⁸² J. P. Sethna, *Statistical Mechanics* **126**, 429 (2011).
- ⁸³ K. Huang and C. H. Holbrow, *Physics Today* **18**, 92 (1963).
- ⁸⁴ Y.-P. Wang, G.-Q. Zhang, D. Zhang, X.-Q. Luo, W. Xiong, S.-P. Wang, T.-F. Li, C.-M. Hu, and J. Q. You, *Phys. Rev. B* **94**, 224410 (2016).
- ⁸⁵ Y.-P. Wang, G.-Q. Zhang, D. Zhang, T.-F. Li, C.-M. Hu, and J. Q. You, *Phys. Rev. Lett.* **120**.
- ⁸⁶ E. Buks, P. Brookes, E. Ginossar, C. Deng, J.-L. F. X. Orgiazzi, M. Otto, and A. Lupascu, *Phys. Rev. A* **102**, 043716 (2020).
- ⁸⁷ D. Dubyna and W. Kuo, *Quantum Science and Technology* **5**, 035002 (2020).
- ⁸⁸ X. Zhang, C.-L. Zou, L. Jiang, and H. X. Tang, *Phys. Rev. Lett.* **113**, 156401 (2014).
- ⁸⁹ E. Mascarenhas, L. Heaney, M. C. O. Aguiar, and M. F. Santos, *Phys. Rev. A* **14**, 043033 (2012).

VII. APPENDIX A

$$H_1 = \begin{pmatrix} N\omega_c - N\mu & \sqrt{N}G_m & 0 & 0 & 0 & 0 \\ \sqrt{N}G_m & (N-1)\omega_c + \omega_m - N\mu & \sqrt{2(N-1)}G_m & 0 & 0 & 0 \\ 0 & \sqrt{2(N-1)}G_m & (N-2)\omega_c + 2\omega_m - N\mu & 0 & 0 & 0 \\ 0 & 0 & \sqrt{3(N-2)}G_m & 0 & 0 & 0 \\ \vdots & \vdots & \vdots & \ddots & \ddots & \vdots \\ 0 & 0 & 0 & 0 & \omega_c + (N-1)\omega_m - N\mu & \sqrt{N}G_m \\ 0 & 0 & 0 & 0 & \sqrt{N}G_m & N\omega_m - N\mu \end{pmatrix}_{(N+1) \times (N+1)} \quad (A1)$$

$$H_2 = \begin{pmatrix} \omega_a + (N-1)\omega_c - N\mu & \sqrt{N-1}G_m & 0 & 0 & 0 \\ \sqrt{N-1}G_m & \omega_a + (N-2)\omega_c + \omega_m - N\mu & \sqrt{2(N-2)}G_m & 0 & 0 \\ 0 & \sqrt{2(N-2)}G_m & \omega_a + (N-3)\omega_c + 2\omega_m - N\mu & 0 & 0 \\ 0 & 0 & \sqrt{3(N-3)}G_m & 0 & 0 \\ \vdots & \vdots & \vdots & \ddots & \vdots \\ 0 & 0 & 0 & 0 & \omega_a + \omega_c + (N-2)\omega_m - N\mu \\ 0 & 0 & 0 & 0 & \sqrt{N-1}G_m & \omega_a + (N-1)\omega_m - N\mu \end{pmatrix}_{N \times N} \quad (A2)$$

VIII. APPENDIX B

$$E_{1,0} = \omega - \mu \quad (B2)$$

The lower excitations eigenvalues are as follows:

$$E_{0,0} = 0 \quad (B1)$$

$$E_{1,-} = \omega - \mu - \sqrt{g_a^2 + G_m^2} \quad (\text{B3})$$

$$E_{1,+} = \omega - \mu + \sqrt{g_a^2 + G_m^2} \quad (\text{B4})$$

$$E_{2,0} = 2(\omega - \mu) \quad (\text{B5})$$

$$E_{2,-'} = 2(\omega - \mu) - \frac{\sqrt{3g_a^2 + 5G_m^2} - \sqrt{30g_a^2G_m^2 + g_a^4 + 9G_m^4}}{\sqrt{2}} \quad (\text{B6})$$

$$E_{2,+'} = 2(\omega - \mu) + \frac{\sqrt{3g_a^2 + 5G_m^2} - \sqrt{30g_a^2G_m^2 + g_a^4 + 9G_m^4}}{\sqrt{2}} \quad (\text{B7})$$

$$E_{2,-} = 2(\omega - \mu) - \frac{\sqrt{3g_a^2 + 5G_m^2} + \sqrt{30g_a^2G_m^2 + g_a^4 + 9G_m^4}}{\sqrt{2}} \quad (\text{B8})$$

$$E_{2,+} = 2(\omega - \mu) + \frac{\sqrt{3g_a^2 + 5G_m^2} + \sqrt{30g_a^2G_m^2 + g_a^4 + 9G_m^4}}{\sqrt{2}} \quad (\text{B9})$$

The parameters involved in Eq. (14) are following:

$$a_1 = -\frac{\sqrt{g_a^2 + G_m^2}}{G_m}, \quad (\text{B10})$$

$$d_1 = \frac{g_a}{G_m} \quad (\text{B11})$$

$$B_1 = 1 + a_1^2 + d_1^2 \quad (\text{B12})$$

$$b = -\frac{\sqrt{30g_a^2G_m^2 + g_a^4 + 9G_m^4} - 7g_a^2 + 3G_m^2}{6\sqrt{2}g_aG_m} \quad (\text{B13})$$

$$c = -\frac{\sqrt{30g_a^2G_m^2 + g_a^4 + 9G_m^4} - 7g_a^2 + 3G_m^2}{6\sqrt{2}g_aG_m} \quad (\text{B14})$$

$$d = -\frac{\sqrt{-\sqrt{30g_a^2G_m^2 + g_a^4 + 9G_m^4} + 3g_a^2 + 5G_m^2}}{2G_m} \quad (\text{B15})$$

$$B_2 = a^2 + b^2 + c^2 + d^2 + 1 \quad (\text{B16})$$

$$a = \frac{\sqrt{-\sqrt{30g_a^2G_m^2 + g_a^4 + 9G_m^4} + 3g_a^2 + 5G_m^2} \left(\sqrt{30g_a^2G_m^2 + g_a^4 + 9G_m^4} - g_a^2 + 3G_m^2 \right)}{12g_aG_m^2} \quad (\text{B17})$$

The second-order corrections to the energy and the normalized eigenstates are following:

$$E_{1,-}^{(2)} = (z\kappa\psi)^2 \left(\frac{\left| \langle \phi_2^{(0)} | \hat{a}^\dagger | \phi_1^{(0)} \rangle \right|^2}{E_{1,-}^{(0)} - E_{2,-}^{(0)}} + \frac{\left| \langle \phi_0^{(0)} | \hat{a} | \phi_1^{(0)} \rangle \right|^2}{E_{1,-}^{(0)} - E_{0,0}^{(0)}} \right) \quad (\text{B18})$$

$$\phi_1^{(1)} = -z\kappa\psi \left(\frac{\langle \phi_2^{(0)} | \hat{a}^\dagger | \phi_1^{(0)} \rangle}{E_{1,-}^{(0)} - E_{2,-}^{(0)}} | \phi_2^{(0)} \rangle + \frac{\langle \phi_0^{(0)} | \hat{a} | \phi_1^{(0)} \rangle}{E_{1,-}^{(0)} - E_{0,0}^{(0)}} | \phi_0^{(0)} \rangle \right) \quad (\text{B19})$$

$$\phi_0^{(1)} = -z\kappa\psi \frac{\langle \phi_1^{(0)} | \hat{a}^\dagger | \phi_0^{(0)} \rangle}{E_{0,0}^{(0)} - E_{1,-}^{(0)}} | \phi_1^{(0)} \rangle \quad (\text{B20})$$

$$\langle \phi_2^{(0)} | \hat{a}^\dagger | \phi_1^{(0)} \rangle = \frac{1}{\sqrt{B_1 B_2}} (d + \sqrt{2}ca_1 + ad_1) \quad (\text{B21})$$

$$\langle \phi_0^{(0)} | \hat{a} | \phi_1^{(0)} \rangle = \frac{1}{\sqrt{B_1}} a_1. \quad (\text{B22})$$